REVIEW OF RESEARCH
IMPACT FACTOR : 5.2331(UIF) UGC APPROVED JOURNAL NO. 48514 ISSN: 2249-894X
VOLUME - 7 | ISSUE - 9 | JUNE - 2018

STUDY OF STRUCTURAL AND MAGNETIC PROPERTIES OF SOL- GEL AUTO COMBUSTIONALLY PREPARED NZF AT DIFFERENT PH VALUES

G. N. Kakade
[1]Department of Physics, R.B.N.B. College, Shrirampur, Ahmednagar,Maharashtra (India).
Corresponding Author: genudaskakade@gmail.com

ABSTRACT :

Nickel – Zinc ferrite particles ($Ni_{0.65}Zn_{0.35}Fe_2O_4$) were prepared at pH values 7,8,9 and10 by using AR grades with high purity (99.99%) nitrates of respective metal ions and L-ascorbic acid as a fuel by sol –gel auto combustion method .The molar ratio of fuel (L-ascorbic acid)to metal nitrates was taken as 1:3.Thes synthesized samples were calcined at 500^{0}C for 6 hrs. These synthesized powder have been characterized by XRD, SEM and impact pH values on the properties of samples were studied. The XRD pattern confirmed that samples were crystalline in nature at pH values 7, 8, 9 and 10 .The crystalline size was found to be 22, 24, 28 and 32nm respectively. The saturation magnetization of samples prepared at pH values 7, 8, 9 and 10 were found 68.74, 71.53, 77.31 and 81.53 a.m.u./g respectively.

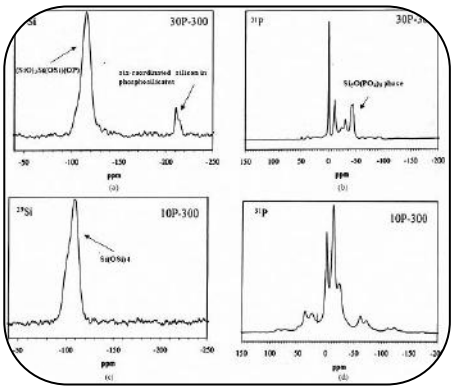

KEYWORDS : *pH of sol-gel, NZF ferrite, XRD, Crystallite size, Magnetic properties.*

1. INTRODUCTION

Spinel ferrite is a kind of soft magnetic material are one of the most attracting class of material due to their interesting electric and magnetic properties. Ni-Zn ferrite is more stable, easily processable ,inexpensive and have wide technological applications[1,2].These are commercially used in the transformer cores, read/write heads for high speed digital tapes and operating devices [3-6].Nickel ferrite is an inverse ferrite whereas zinc ferrite is normal so it is interesting to study their magnetic properties .Magnetic properties of these ferrite are highly sensitive to preparation technique, sintering condition and amount of constitutes metal oxides, impurities or doping level [7].Generally Ni-Zn ferrites are synthesized using conventional solid state reaction i.e. ceramic method [8-11] which involves direct mixing of oxides, prolonged heating at high temperature is mainly disadvantage of this method giving rise the vitalization of some constituents and non-stoichiometric product. The particles obtained by this method are large and non-uniform in size which results in the formation of voids on compacting. A variety of methods have been proposed for the synthesis of Ni-Zn ferrite nanoparticles with control size, shape, and chemical stability such as sol-gel method12],thermal combustion method[13],citrate precursor route[14],co-precipitation method[15], thermal plasma synthesis,[16], reverse micelle [17,18],hydrothermal[19],micro-emulsion[20],and sonochemical reaction [21]. Sol-gel method, which is one of the most useful and attractive technique for the synthesis of nanosized ferrites because of its advantages such as; good stoichiometric control and the production of ultrafine particles, with a narrow size distribution in a relatively short

processing time at a very low temperature [22].The size of the particles can be varied by changing the solution composition, pH, and calcination temperature [23].

In present work NZP nanoparticles were prepared by changing pH and effect of pH on properties was studied.

2. EXPERIMENTAL PROCEDURE

Synthesis of Ni-Zn ferrite nanoparticles

Sol–gel auto combustion method was employed to synthesize Ni–Zn ferrite system having composition of $Ni_{0.65}Zn_{0.35}Fe_2O_4$ In the synthesis of Ni-Zn spinel ferrites, AR grades with high purity (99.99%) nitrates of respective metal ions (Nickel, Zinc and Ferric) were used and L-Ascorbic acid was used as a fuel for the synthesis. All nitrate and L-ascorbic acid were first dissolved in minimum amount of double distilled water. The molar ratio of fuel (L-ascorbic acid) to metal nitrates was taken as 1:3. This initial solution was highly acidic and having pH\1. Ammonia was added to adjust different pH values (7, 8, 9 and 10) of the initial solution. These solutions were evaporated at 75 °C to get a dense sticky gel; the temperature was increased to 110 °C for the dehydration process. The temperature was then increased rapidly and when it reached approximately 120 °C, large amounts of gases (CO_2, H_2O, and $N2_)$ were liberated, and a dark brown ferrite powder was produced through the combustion process. Finally, the as-burnt powder was calcined at 500 °C for 6 h with a heating rate of 5 °C/min to obtain the Ni-Zn ferrite nanoparticles.

3. CHARACTERIZATIONS

Structural characterization

Phase formation of the cubic spinel structure samples was examined by X-ray diffraction (XRD) pattern obtained using Rigaku Corporation, Japan diffractometer at room temperature. The pattern was recorded using Cu-Kα radiation (λ=1.54182 Å) in the 2θ range 20° – 80° with step size 0.02° and time/step 2 s. Structural information such as the present phases, lattice parameter, and crystallite size can be extracted from the samples diffraction patterns.

Morphological characterization

The surface morphological studies were carried out using scanning electron microscopy using JEOL JSM-6360 scanning electron microscope (SEM).

Magnetic Measurement

The magnetic properties of the Ni-Zn spinel ferrite nanoparticles were investigated using pulse field hysteresis loop technique at room temperature.

4. RESULTS AND DISCUSSION

Structural properties

4.1 X-ray diffraction study

Fig. 4.1 (a-d) shows the X-ray diffraction pattern $Ni_{0.65}Zn_{0.35}Fe_2O_4$ samples synthesized at different pH values (7, 8, 9 and 10). X-ray diffraction analysis revealed that all the diffraction peaks seen in the XRD pattern well matches with the standard pattern of pure nickel ferrite. The analysis of XRD pattern revealed the formation of single phase cubic spinel structure. The peaks of the XRD patterns were corresponding to (220), (311), (222), (400), (422), (511) and (440) planes. The width of diffraction maxima peaks (311) becomes reduced and intensity of peaks increased as the increases. The intensity of (311) plane is more as compared to other planes like (220), (222), (400), (422), (511) and (440).

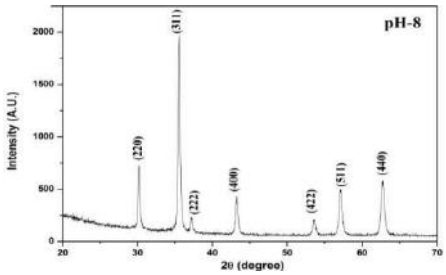

Fig 4.1(a)XRD pattern of NZP nanoparticles for pH-7

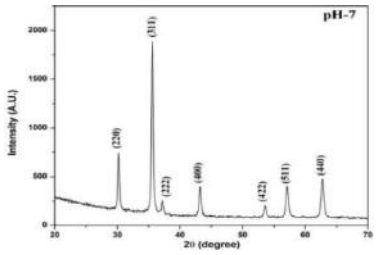

Fig. 4.1(b): XRD pattern of NZP for nanoparticles for pH-8

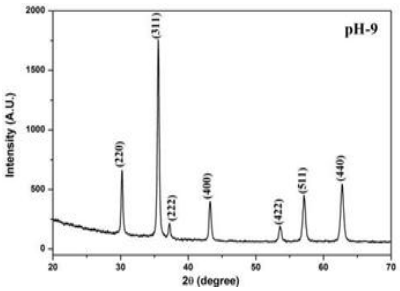

Fig. 4.1(c): XRD pattern of NZP nanoparticles for pH-9

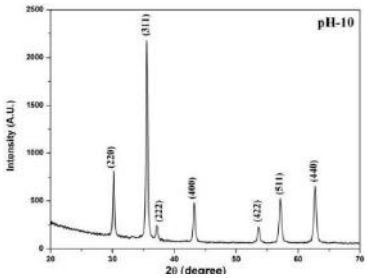

Fig. 4.1 (d): XRD pattern of NZP nanoparticles for pH-10

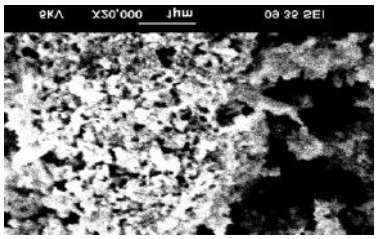

Fig. 4.2 (a): SEM image of NZP nanoparticles for pH-7

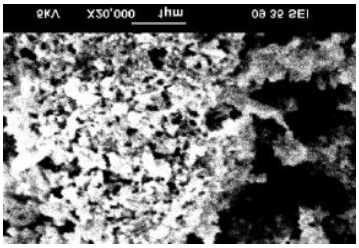

Fig. 4.2 (b): SEM image of NZP nanoparticles for pH-8

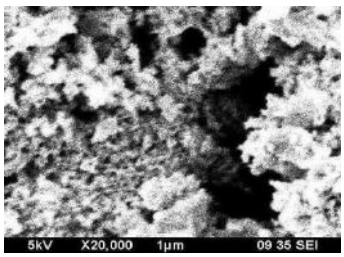

Fig. 4.2 (c): SEM image of NZP nanoparticles forpH-9

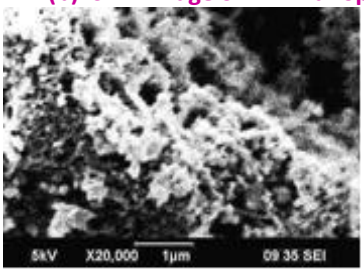

Figure 4.2 (d) : SEM image of NZP nanoparticles forpH-10

The lattice constant value 'a' (Å) of $Ni_{0.65}Zn_{0.35}Fe_2O_4$ nanoparticles synthesized at different pH was determined by using the relation [24],

$$a = d_{hkl}\sqrt{h2+k2+l2}$$

Where, (a) is the lattice constant, (d) is the interplanar spacing; (h k l) is the Miller indices. The obtained values of the lattice constant (a) are tabulated in Table 4.1. There is slight changes were observed for lattice constant '*a*' which could be associated with the Slight changes were observed for lattice constant

'*a*' which could be associated with the pH solution. The results presented in Table 4.1 show that the lattice parameters a, b and c agree with the equation a = b = c, indicating that the prepared sample belongs to cubic lattice. The average crystallite size of $Ni_{0.65}Zn_{0.35}Fe_2O_4$ nanoparticles synthesized at different pH (pH-7, 8, 9 and 10) was determined using the relation [25], $t = \frac{0.9\lambda}{\beta cos\theta}$ Where, β is the full width at half maximum (FWHM) and (1.5403 Å) is wavelength of the target material.

The obtained values of the crystallite size are tabulated in Table 4.1. Using the Scherer's formula, the variations of full-width at half maximum (FWHM) at different XRD peaks indicated that the average crystallite size of the nanoparticles were about 22, 24, 28 and 32 nm corresponding to the pH of 7, 8, 9 and 10, respectively. The average crystallite size is increased as the pH increases. Due to the rapid combustion rate and high flame temperature with increasing pH, higher pH produces larger crystallite size and good crystallinity It has been experimentally observed by some researchers that nanocrystalline powders are quite susceptible to the formation of inter-particle London– van der Waals bonds either in the wet or in the dry state due to their very fine particle size [26]. The X-ray density (dx) of $Ni_{0.65}Zn_{0.35}Fe_2O_4$ nanoparticles synthesized at different pH (pH -7, 8, 9 and 10) was calculated by using the relation [27],

$d_x = \frac{Z \times M}{V \times NA}$ gm /cm^3 where, Z is the number of molecules per formula unit (Z = 8 for spinel system), M is molecular mass of the sample, V is the unit cell volume; N_A is the Avogadro's number.

The X-ray density depends on the molecular weights of the samples and lattice constants.

The X-ray density values are tabulated in Table 4.1; the obtained values of X-ray density are in reported range, which are depends on lattice constant, therefore same nature of lattice constant observed in the X-ray density value with increase pH of sample. The value of volume of unit cell value determined from cube of lattice constant, which indicate that the volume of the unit cell depends on the lattice constant, therefore same nature of lattice constant observed in the volume of unit cell values with increase pH of sample.

'Ph maintain at	A (Å)	d_x (gm/cm^3)	V (Å^3)	Crystallite size (t)
pH-7	8.3640	5.3748	585.557	22
pH-8	8.3678	5.3671	586.334	24
pH-9	8.3603	5.3825	584.759	28
pH-10	8.3667	5.3690	586.103	32

Table 4.1: Lattice parameter (a), X-ray density (d_x), Unit cell volume (V) and Crystallite size (t) of $Ni_{0.65}Zn_{0.35}Fe_2O_4$ nanoparticles (pH-7, 8, 9 and 10).

Various other structural parameters like hopping lengths (L_A, L_B), tetrahedral bond length (d_{AX}), octahedral bond length (d_{BX}), tetra edge (d_{AXE}) and octa edge (d_{BXE}) were evaluated from following relation for different pH value [28, 29].

$L_A = a\sqrt{(3)}/4$ Å

$L_B = a\sqrt{(2)}/4$ Å

$d_{AX} = a(3(u-1/4))^{1/2}$ Å

$d_{BX} = a[3u^2-(11/4)\ u+(43/64)]^{1/2}$ Å
$d_{AXE} = a[2(2u-1/2)]^{1/2}$ Å
$d_{BXE} = a[2(1-2u)]^{1/2}$ Å
$d_{BXEU} = aV\ (4u^2-3u+11/16)$ Å

Using the values of the lattice constant (a), the various other structural parameters like hopping lengths (L_A, L_B), tetrahedral bond length (d_{AX}), octahedral bond length (d_{BX}), tetra edge (d_{AXE}) and octa edge (d_{BXE}) were evaluated from XRD data for different pH value and indexed in Table 4.2. The obtained structural parameters aredepends on lattice constant values, there were no increasing or decreasing trend observed in the hopping lengths (L_A, L_B), tetrahedral bond length (d_{AX}), octahedral bond length (d_{BX}), tetra edge (d_{AXE}) and octa edge (d_{BXE}) values with increasing pH value of Ni-Zn sample.

'pH' maintain at	L_A (Å)	L_B (Å)	dAX (Å)	dBX (Å)	dAXE (Å)	dBXE (Å)	
						Shared	Unshared
pH-7	3.6217	2.9571	1.8978	2.0420	3.0911	2.8152	2.9588
pH-8	3.6235	2.9585	1.8987	2.0430	3.1005	2.8165	2.9602
pH-9	3.6200	2.9557	1.8969	2.0411	3.0976	2.8138	2.9574
pH-10	3.6230	2.9582	1.8985	2.0428	3.1002	2.8162	2.9599

Table 4.2: Hopping length (L_A, L_B),Tetrahedral bond (d_{AX}), Octahedral bond (d_{BX}), Tetra edge (d_{AXE}) and Octa edge (d_{BXE}) of NZP nanoparticles (pH-7, 8, 9 and 10).

The tetrahedral A-site ionic radii can be calculated using the value of lattice constant 'a' and oxygen positional parameter 'u' (u = 0.381Å) as

$$r_A = (u-\frac{1}{4})\, a\sqrt{3} - r\,(O^{2-})\, A^0$$

where, '$r_{A'}$ represents radius of tetrahedral (A) site cation, 'u' oxygen positional parameter, 'O' represents radius of oxygen anions. The octahedral B-site ionic radii can be calculated using the equation:

$$r_B = (\frac{5}{8} - u)\, a - r\,(O^{2-})\, A^0$$

Where, r_B represents radius of octahedral [B] site cation.

The values of tetrahedral (A-site) and octahedral [B-site] of ionic radius are given in Table 4.3. The values of tetrahedral (A-site) and octahedral [B-site] value depends on the values of lattice constant, therefore, it is found that obtained values tetrahedral (A-site) and octahedral [B-site] are in reported range. There are no more changes observed in tetrahedral and octahedral ionic radii values with increasing pH of sample [30, 31].

'pH' Maintain at	r_A (Å)	r_B (Å)
pH-7	0.5778	0.7208
pH-8	0.5787	0.7218
pH-9	0.5769	0.7198
pH-10	0.5785	0.7215

Table 4.3: Ionic radii (r_A, r_B) of $Ni_{0.65}Zn_{0.35}Fe_2O_4$ nanoparticles (pH-7, 8, 9 and 10).

MORPHOLOGICAL ANALYSIS

4.2 Scanning electron microscopy (SEM)

Surface morphology and average grain size of the $Ni_{0.65}Zn_{0.35}Fe_2O_4$ (pH- 7, 8, 9 and 10) nanoparticles were determined by using scanning electron microscope technique by

Surface morphology and average grain size of the $Ni_{0.65}Zn_{0.35}Fe_2O_4$ (pH- 7, 8, 9 and 10) nanoparticles were determined by using scanning electron microscope technique by selecting 35,000 magnification ranges. Fig. 4.2 (a-d) shows the SEM images of the Ni-Zn ferrites synthesized at different pH. The SEM images show clearly the change in morphology as the pH of the solution increases from 7 to 10. By increasing the pH value, the average grain size decreases to some extent. The formation of pores and voids in the samples can be attributed to the release of large amounts of gases during the synthesis combustion process since the rate of combustion is increased significantly with increasing pH values. The average grain size (89-74 nm) is slightly decreased with increasing pH values. This is probably associated with the use of ammonia which is used to vary the pH value. Typically, the degree of hydrolysis increases significantly with the intensification of pH value and during the combustion process, the metal hydroxide converts to crystal easier than un-hydrolysed water-dissolving metal salt. However, when the pH increases, the growth in truncated octahedron shape gradually increases. Hence, the grain size seems to be smaller as the pH increases. Faster rate of solidification could occur at higher pH values during sintering, resulting in more nucleation points and smaller grains. Additionally the SEM micrograph shows the grain growth is porous and irregular. The micrographs show irregular size of the particles along with more agglomeration. Furthermore, the agglomeration of particles is attributed to the interaction between magnetic particles. The effect of pH on the microstructure of Ni-Zn ferrite nanoparticles can be explained in terms of the increase pore mobility due to the creation of excess cation vacancies [32]. The average grain size was determined using the linear intercept method estimated using the relation [33],

$$Gavg = \frac{1.5L}{MN}$$

Where, *L* is the total test line length, *M* is the magnification and *N* the total number of interception.

The grain size of the samples ($Ni_{0.65}Zn_{0.35}Fe_2O_4$ (pH- 7, 8, 9 and 10) were estimated by counting a sufficiently large number of grains to ensure accuracy using linear intercept method Average grain sizes are found to be in the nano regime from 89-74 nm. The average grain size and corresponding specific surface area to volume ratio are tabulated in Table 4.4

'pH'maintain at	Grain Size (nm) SEM	Specific surface area (m2/g)
pH-7	89	12.54
pH-8	78	14.33
pH-9	76	14.67
pH-10	74	15.10

Table 4.4 Grain size (G), specific surface area (S) from typical scanning electron microscopy (SEM) image for NZP nanoparticles (pH-7, 8, 9 and 10). nanoparticles

4.3. Magnetic Properties

Pulse field hysteresis loop technique

The magnetic properties of the $Ni_{0.65}Zn_{0.35}Fe_2O_4$ nanoparticles synthesized at different pH (pH-7, 8, 9 and 10) were measured using a pulse field hysteresis loop tracer technique for the applied field of 6000 Oe at 300 K. The magnetic properties of the nanoparticles depend on the microstructure and measuring parameters, such as particle size, porosity, and magnetizing frequency. Fig. 4.3 (a-d) shows the magnetic hysteresis loops $Ni_{0.65}Zn_{0.35}Fe_2O_4$ ferrite nanoparticles with different pH value at room temperature. The hysteresis loops were measured to determine parameters, such as the saturation magnetization (Ms), remnant magnetization (Mr), and coercivity (Hc), are shown in Table 4.5. The magnetic properties of the samples clearly depend on the size of the nanocrystallities. It is evident from Table 4.5 that the saturation magnetization (Ms) increases with increasing pH value. The decrease in saturation magnetization (Ms) can be attributed to increase of the mean size of nanocrystallities from the analysis of M-H loop, it can be seen that the M–H loops are well saturated at this applied field and the minimal hysteresis area indicates that the $Ni_{0.65}Zn_{0.35}Fe_2O_4$ is a soft magnetic material.

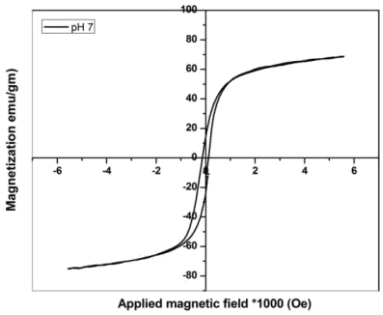

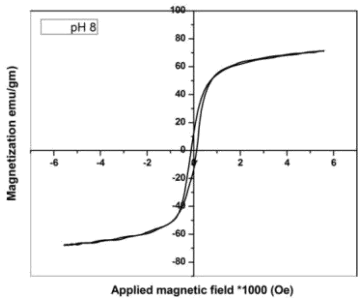

Fig. 4.7 (Fig.4.3 (a): M-H plots for NZP nanoparticles for (pH 7) **Fig. 4.3 (b): M-H plot for N_{ZP} nanoparticles for (pH 8)**

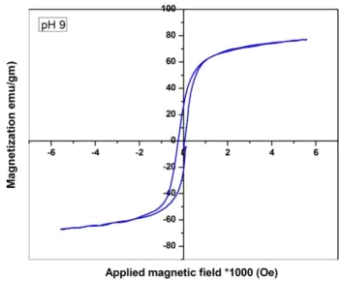

Fig.4.3 (c): M-H plot for NZP_4 nanoparticles for (pH 9)

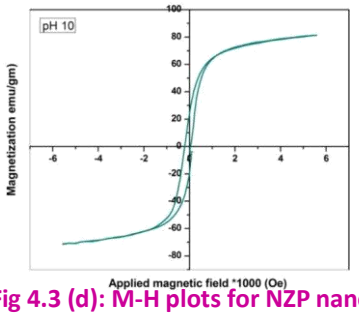

Fig 4.3 (d): M-H plots for NZP nanoparticles for (pH 10)

The values of magneton number nB (saturation magnetization per formula unit in Bohr magneton) were obtained from hysteresis loop. The magnetic properties of $Ni_{0.65}Zn_{0.35}Fe_2O_4$ nanoparticles synthesized at different pH are listed in Table 4.5. It can be seen from the Table 4.5 that the values of saturation magnetization (Ms), remnant magnetization (Mr), coactivity (Hc) and anisotropy constant (K) are varying with pH, which may be due to the difference of particle size and their morphology. Such kinds of variations were also observed by Yu and Liu [34]. They have also reported the effect of different pH on the particles size, morphology and subsequently on the magnetic properties of the ferrites synthesized at different temperature. The variation in pH during the synthesis process is expected to change the size and structural morphology of the nanoparticles, which ultimately causes the variation in the values of magnetic parameters such as; Ms, Mr and Hc Wu et al. Since pH is an important factor during synthesis, the degree of chelation of metallic ions can be controlled by adjusting the pH of the starting solution. Increasing/decreasing the pH can increase or decrease the degree of chelation of metallic ions in the solution and it affect the chemical reactions, which basically influence the overall growth of the nanoparticles? Yue et al., have also investigated the effect of pH of the precursor solutions on the structure of dried gels.

pH' maintain at	MS (emu/g)	Mr (emu/g)	HC (Oe)	Mr/MS	nB
pH-7	68.74	14.35	119.01	4.790	0.608
pH-8	71.53	13.20	118.33	5.418	0.560
pH-9	77.31	17.25	140.65	4.482	0.731
pH-10	81.53	11.40	111.83	7.150	0.483

Table 4.5: Saturation magnetization (Ms), Remanence magnetization (Mr), coercivity (H_C), Remanence ratio (Mr/Ms) and Magneton number (n_B) of NZP nanoparticles (pH-7, 8, 9 and 10

It was observed that high porous precursors with network structure can be formed at high pH values which affect the combustion behaviour of the gel. The porous network structures make the materials burn rapidly and violently. With increasing pH value, the combustion rate was increased significantly. They observed that the as-burnt powders become uniform in size and the crystallites size was increased from 22 to 32 nm by increasing pH from 7 to 10. Ferrites of higher density and permeability can be also prepared from the solutions by varying the pH values. Thus, the variation in pH during the synthesis may be expected to affect the growth of the nanoparticles and consequently the magnetic properties. It is because of the fact

that the magnetic behaviour of the nanoparticles evolve through the competition between the shape anisotropy and size of the nanoparticles [35].

5. CONCLUSION

Nanocrystalline Ni-Zn ferrite has been synthesized at different pH via Sol-gel auto combustion method, which is characterized on nanosized shape etc. by X-Ray diffraction. The particle size is in the range of 22-32 nm. The prepared Ni-Zn samples annealed at temperature 500 °C for 2 hr is formed a good crystalline cubic phase spinel structure. The crystallite size is in the range on 74-89 for different pH values. With increase in pH from 7 to 10 the crystallite size decreases. The surface morphology of the prepared samples is strongly influenced by pH. The grain size obtained from SEM images show decreasing trend with increasing pH.The saturation magnetization obtained from M-H plot show decreases with increase in pH.

ACKNOWLEDGEMENT

The author are very thankful to Dr.K.M.Jadhav,Professor ,Department Physics,Dr.Babasaheb Ambedkar Marathwada University Aurangabad, (M.S.),India for their fruitful guidance and for providing laboratory facilities.

REFERENCES

[1] M.Sugimoto: *J.Am.Ceram.Soc*., 82 (2)(1999).269
[2] A.M.Abdeen: *J.Mag.Mag.Mater.,* 185 (1998).199
[3] A.M.Abdeen: *J.Mag.Mag.Mater.*192 (1999)121.
[4] H.Igarash, K.Okazaki:*J.Am.Ceram.Soc.,* 60 (1977)51
[5] J.Kullikowski: *J.Mag.Mag.Mater.,* 41 (1984)56.
[6] P.Ravindranath, K.C.Patil:*J.Mat.Sci.,* 22 (1987)3261
[7] O.F.Caltum,L.Spinu:*IEEE Trans Mag.,*37(2001)2353.
[8] E. Rezlescu, N.Rezlescu,C.Posnicu,M.L.Crauss:*Ceramic Int.*,19(1993)139
[9] N. Rezlescu, E.Rezlescu: *Solid State Comm.,* 88(1993)139.
[10] M.C.Sable, B.K.Labde, N.R.Shamkumar:*Bult.Mater.Sci.* 28 (2005)35.
[11] A.A.Sattar,H.M.EI Sayad,K.M.EI Shotrofy,M.M.EI Tubey:*J.Appl.Sci.,*5(2005)35.
[12] B.T.Naughton,P.Majewski,D.R.Clarke: *Journal of the American Ceramic Society.*,Vol. 90(2007),3547-3553
[13] E.E.Sileo,R.Rotelo,S.E.Jacobo;Physica B:*Condensed Mater.,*Vol 320 (2002) 257-260
[14] R.K. Singh,C.Upadhyay,S.Layek,A.Yadav;*International Journal of Engineering , Science and Technology,* Vol.2 (2010) 104-109.
[15] K.Velmurugan,V.S.K.Venkatachlapathy,S.Sendhilnathan;*Material Research.*,Vol.13 (2010) 299-303.
[16] M.Shigeta,A.B.Murphy; *Journal of Physics D:Applied Physics.*,Vol,44 (2011) ,Article ID: 174025
[17] S, A, Morrison, C.L.Cahill,E.E.Carpenter,S.Calvin,R.Swaminathan,M.E.McHenry,V.G.Harris;*Journal of Applied Physics* .Vol.95 (2004), Article ID: 6392.
[18] S.Thakur, S.C.Katyal, A.Gupta, V.R.Reddy,S.K.Sharma,M.Knobel,M.Singh;*Journal of Physical Chemistry C*, Vol.113,(2009) 20785-20794.
[19]P.E.Meskin,V.R.IvanovA.E.Barantchikov,B.R.Churangulov,Y.D.Tretyakov; *Ultrasonics Sonochemistry,Vol,* 13(2006) 47-53.
[20] D.Mathew,R.Juang; *Chemical Engineering Journal*,Vol,129,(2007) 51-65.
[21]M.G.Naseri,E.B.Saion,M.Hashim,A.H.Shaari,H.A.Ahangard;*SolidStateCommunication*,Vol.151,(2011), 1031- 1035.
[22] M.Srivastava, S.Chaubey, K.O.Animesh; *Mater.Chem.Phy.*118 [1] (2009), 174-180.
[23].Satyanarayan,K.Madhusudan Reddy,S.V.Manorama;*Mater.Chem.Phys*.82[1] (2003), 21-26.
[24]P.P.Khirade,S,D,Birajdar,A.V.Humbe,K.M.Jadhav*; Journal of Electronicterial,*45 (2016)3227-3235

[25]M.Rajendra, R.Pullar,ABhattacharya,D.Das,S.Chintalapudi,C.Majumdar;*Journal of Magnetism and Magnetic Materials*,323(2001)71-83
[26]H.Hamaker, Physica, 4(1937)1058-1072
[27]R.Kamble,P Shaikh,S.KambleY.Kolekar;*Journal of Alloys and Compound,*478 (2009), 599-603
[28] Vinayak, P.P. Khirade, S.D. Birajdar, P. Gaikwad, N. Shinde, K. Jadhav;, *Int. Adv. Res. J. Sci. Eng. Technol*., 2 (2015) 55-58.
[29] S. Sindhu, D. Birajdar; *IOSR Journal of Applied Physics* 3 (2013) 33-41.
[30] A. El-Sayed; *Ceramics International*, 28 (2002) 363-367.
[31] P. Priyadharsini, A. Pradeep, P.S. Rao, G. Chandrasekaran,; *Materials Chemistry and Physics*, 116 (2009) 207-213.
[32] K. Janghorban, H. Shokrollahi;*Journal of magnetism and magnetic materials,* 308 (2007), 238- 242.
[33]A.Thorvaldsen, ; Acta materialia, 45 (1997) 595-600.
[34]X. Liu, W. Zhong, S. Yang, Z. Yu, B. Gu, Y. Du,**;** *Journal of Magnetism and Magnetic Materials,* 238 (2002) 207-214.
[35]S. Rusponi, T. Cren, N. Weiss, M. Epple, P. Buluschek, L. Claude, H. Brune,; *Nature Materials*, 2 (2003) 546-551.